Computationally led high pressure synthesis and experimental thermodynamics of rocksalt yttrium monoxide

B.L. Brugman[1], Y. Han[1], L.J. Leinbach[2], K.D. Leinenweber[2], A. van de Walle[3], S.V. Ushakov[1], Q.-J. Hong[4,*], and A. Navrotsky[1,4,*]

[1]Navrotsky-Eyring Center for Materials of the Universe, School of Molecular Sciences, Arizona State University, Tempe, AZ 85287

[2]Eyring Materials Center, Arizona State University, Tempe, AZ 85287

[3]School of Engineering, Brown University, Providence, RI 02912

[4]Ira A. Fulton School for the Engineering of Matter, Transport and Energy, Arizona State University, Tempe, AZ 85287

Abstract

Yttrium monoxide (YO) is a possible member of a large family of rare earth monoxides having the rock salt structure. It was predicted to be stable above 10 GPa and to be superconducting with higher critical temperatures at lower pressures. However, no syntheses of bulk YO have been reported. Using first principles calculations, we predicted the stability of yttrium monoxide at pressures above 8.6 GPa and at high temperature. Guided by these predictions, we successfully synthesized bulk YO in the rock salt structure (*Fm*-3*m*) at 15 GPa and 1600 °C. YO is very metastable (both thermodynamically and kinetically) at ambient conditions and decomposes rapidly on heating. Our combined experimental and computational approach enabled us to obtain consistent results for the formation enthalpy and lattice constant of bulk YO. The predicted enthalpy of formation for the reaction $Y + Y_2O_3 = 3YO$ is 32.7 kJ/mol, and experiments yield a value of 35.7 kJ/mol, with an estimated uncertainty of ± 5 %. YO in the rock salt structure has a refined lattice constant of 4.872 ± 0.008 Å and a molar volume of 17.41 ± 0.08 cm^3 mol^{-1}. From these, we calculated the entropy and *P-T* slope of the reaction. Through this comprehensive investigation, we explored the synthesis and decomposition of a challenging metastable phase which is stabilized under high pressure conditions. Moreover, we have gained valuable insights into the thermodynamics and physical properties of YO. These findings highlight the importance of leveraging pressure as an additional dimension in materials synthesis and underscore the potential of using first principles calculations to guide experiments involving highly metastable materials.

**Corresponding authors: A. Navrotsky anavrots@asu.edu and Q. Hong qhong7@asu.edu*

Introduction

Rare earth (RE) oxides and their thermodynamics are important in applications ranging from superconductors to lasers to thermal barrier coatings and ceramics[1–5]. The term RE includes lanthanide metals, but also may be extended to scandium and yttrium [1,6]. The inclusion of yttrium containing oxides with other rare earth oxides has led to important discoveries. Substituting Y in rare earth barium copper oxide (REBCO, to obtain YBCO) compounds resulted in the discovery of the first superconductor with a critical temperature above the boiling point of liquid nitrogen[3], and yttrium garnets with aluminum and iron (YAG and YIG), often doped with other lanthanides, are important optical and magnetic materials[2,7,8].

Rare earth monoxides (REO) also exhibit interesting electronic and magnetic properties[9–14], and are potentially important analogs for understanding the properties of actinide oxides[15]. Though their nominal stoichiometry tempts one to assign a valence of two to the RE, their actual electronic states and electrical conductivity are more complex[9,16]. REO are interesting for spintronics, and potentially useful as conductors and ferromagnetic semiconductors[14,17–20]. Further, LaO is superconducting and YO is a tunable semiconductor at ambient conditions[16,21]. Rock salt YO was predicted to be a superconductor with the highest critical temperature (T_C) = 13 K[22]) among simple binary oxides. The predicted T_C for YO increases as pressure decreases[22]. Experimental work on bulk phases of YO as well as other REO, is needed to explore potential superconductivity, as well as other physical properties.

Monoxides of several rare earth metals – LaO[23,24], CeO[25], NdO[26], SmO[27,28], EuO[28] and YbO[29] – were initially synthesized in the mid twentieth century[30], though many early syntheses were ultimately found to produce carbides or nitrides[9,28,31]. Successful synthesis of these REO was achieved at high pressure in the 1980s, though the feasibility of high pressure synthesis of the remaining REO was questioned[9,32]. More recently, epitaxial thin films of many REO have been synthesized at ambient pressure[9,14,16,21,32–35].

The successful synthesis of pure bulk YO has not been previously documented, but YO was reported once in the 1950s as an impurity in combustion experiments with metallic yttrium[36]. YO is one of a group of yttrium oxide stoichiometries recently predicted to form under high pressure conditions[22], and synthesis of phase pure bulk YO, along with measurement of its structural, physical, and thermodynamic properties, offers a challenge addressable by a combination of computational and experimental methods and defines the emphasis of this paper.

Here we combine density functional theory (DFT) and lattice dynamics calculations with high pressure synthesis and experimental thermochemical measurements to predict and characterize bulk YO formation and energetics. Guided by insights gained from the calculations, pure YO was successfully synthesized in a multi-anvil press at 15 GPa and 1600 °C (**Figure 1**). Differential scanning calorimetry (DSC) with complementary high temperature oxide melt solution calorimetry and fast scanning differential scanning calorimetry (FDSC) was used to measure the decomposition energetics of bulk YO, which were used to construct a preliminary *P-T* boundary for the reaction $Y + Y_2O_3 = 3YO$. The extreme metastability of YO on heating at ambient pressure required careful analysis of calorimetric data, guided by the constraints from computation, to obtain consistency among different measurements. This multifaceted approach will be generally applicable to other highly metastable materials.

Experimental Methods

Calculations. We employed first-principles density functional theory (DFT)[37,38] to model Y, Y_2O_3, and YO. The electronic structures were calculated using the Vienna Ab initio Simulation Package (VASP)[39,40], with the projector-augmented-wave (PAW)[41] implementation. The exchange-correlation energy was determined using the generalized gradient approximation (GGA), in the form known as Perdew–Burke–Ernzerhof (PBE)[42]. The pseudopotentials used were the Y_sv pseudopotential, with the inner core 4s and 4p electrons relaxed, and standard O pseudopotential.

Under the quasi-harmonic approximation, we performed lattice dynamics calculations using the ATAT package[43]. The Gibbs free energy for the reaction Y (*P63/mmc*) + Y_2O_3 (C-type) = 3YO (rocksalt) was computed at 0 Kelvin at pressures of 5, 10, 15 and 20 GPa and values at each pressure are presented in **Figure 2**.

High pressure synthesis. Y_2O_3 powder (99.9 %, Alfa Aesar) was annealed at 1000 °C immediately before transfer to a nitrogen filled glovebox. Y metal (99.6 % (metal), mesh 40, Alfa Aesar) was received packed under Ar and opened in the glovebox. The phase analysis of Y metal was performed by XRD in a sealed holder. Y was confirmed to be in the hexagonal P63/mmc phase. The particle size <420 μm (40 mesh) was chosen based on our observation that higher purity Nd and Y metals with smaller particle size from the same supplier were in fact fluorite type metal

hydrides, and, if used as a precursor for high pressure synthesis, produced oxyhydrides rather than rock salt monoxides.

Y metal and Y_2O_3 were mixed in nominal stoichiometry $YO_{0.96}$ to account for possible surface oxidation of Y metal. The powders were loaded into either a 3 mm or 2 mm cubic boron nitride (cBN) capsule. Compression experiments were conducted in a multi-anvil press either 14/8 or 10/5 injection molded 55 wt % MgO/spinel octahedral pressure media[44]. The assemblies were compressed in WC cubic anvils with the {111} faces truncated to 8 mm or 5 mm dimensions. For all experiments in which YO was synthesized, pressure was increased to 10-15 GPa over 12-24 hours, and the assembly was heated to 1200-1600 °C and held for 1-5 hours. Temperature was measured directly by a type C thermocouple when the thermocouple functioned well, or estimated by power across the sample heating leads when it did not. After heating, power was cut to the heater resulting in quenching to ambient temperature over a few seconds and the pressure was reduced to ambient conditions over ~10-12 hours. The recovered capsules were opened and the YO sample pellet was cleaned minimally by breaking or scraping off remaining large pieces of the capsule to remove residue and minimize impurity. The sample was then moved to a nitrogen atmosphere. The optimal experimental conditions for high temperature synthesis were 15 GPa and 1600 °C. Experiments are tabulated in supplementary **Table S1**.

X-ray diffraction. A Bruker D2 diffractometer using Cu Kα radiation and a 1 mm scattering shield was used to collect X-ray diffraction patterns from sample pellets. Pellets were transferred to an atmospherically controlled holder. XRD was collected directly from the sample pellet without powdering to avoid back-transformation. Lattice parameters were determined with GSAS II software[45] using an NdO crystallographic information file (CIF) file generated by Materials Project[46] and modified for YO. The NIST Si standard 640C was used to calibrate initial instrument parameters. Lattice parameter and the sample displacement parameter were simultaneously refined to accommodate for the YO pellet morphology. Microstructure was also refined to profile the peak shape for unpowdered samples quenched from high pressure. Atomic positions and interatomic distances for YO are provided in supplementary **Table S2**, and a CIF for YO is included as supplementary material. Refinement results for a 15 hour scan of the approximately pure phase synthesized at 15 GPa and 1600 °C are presented in **Figure 3**. The weighted residuals (wR) for the fit from the long scan are 2.21 %, with a goodness of fit (GOF) value of 1.77. For shorter scans on

all phase pure samples, the mean of the wR is 4.44 ± 0.94 % (see **Table S3** for lattice parameter and microstructure refinement results).

Calorimetry. High temperature oxide melt solution calorimetry was conducted in a Setaram AlexSYS calorimeter at 800 °C in sodium molybdate ($3Na_2O{\cdot}4MoO_3$) solvent. The calorimeter was calibrated with 5 mg benzoic acid pellets ($C_7H_6O_2$ Sigma). YO pellets were dropped from room temperature conditions. The dropping tube atmosphere was constantly flushed with dry air (ProSpec) at a rate of 80 mL/min, and the solvent was stirred by bubbling air at ~35 mL/min. Methodological details and design of the drop solution calorimeters are described elsewhere[47,48]. Thermochemical cycles for dissolution and oxidation to Y_2O_3 are given in the supplementary information in **Table S4** and **Table S5**. Tabulated enthalpy results are given in **Table S6**.

Differential scanning calorimetry was conducted under vacuum in a Setaram SenSys calorimeter coupled to the vacuum system of Micromeritics ASAP 2020 adsorption instrument. A 5.52 mg pellet of YO was degassed and heated to 550 °C at 10 °C/min in the low atmosphere environment. The vacuum was maintained on cooling to prevent oxidation of decomposition products. A sharp, well defined exothermic peak was observed at 180 °C during heating. No peaks were observed during the cooling cycle. The sample was weighed and the mass after cooling was 5.35 mg, suggesting no oxidation occurred during the heating and cooling cycle. XRD patterns were collected before and after calorimetry experiments (supplementary **Figure S2**).

Fast scanning differential scanning calorimetry (FDSC) was conducted in a Mettler Toledo Flash DSC2+ on a UH1 high-temperature chip (Xensor). A scanning rate of 1000 °C/s was used to measure heat flow on an unweighed sample with areal dimensions <100 μm. The sample was scanned under Ar with a flow rate of 20 mL/min. Two sharp peaks were observed at 280 °C and 430 °C on heating. No peaks were observed on cooling or on subsequent heating and a total of three heating and cooling cycles were conducted and confirmed that reactions were not reversible.

Results and Discussion

To predict free energies of formation of YO in the *Fm*-3*m* structure from Y and Y_2O_3 as a function of pressure, we employed DFT lattice dynamics calculations. Our calculations reveal that YO is metastable by 32.7 kJ/mol under ambient pressure and is predicted to become stable above 8.6 GPa, as illustrated in **Figure 2**. The result compares favorably with other computational work predicting stability at 9.9 GPa[22]. This analysis allowed us to investigate the effects of pressure on

the reaction and provided us with the lattice parameter for rock salt YO. These predictions support the potential synthesis of YO and suggest recoverability of metastable YO on quenching to ambient conditions.

Recovery was indeed achieved for essentially pure YO when synthesized in the multi-anvil press at 15 GPa and 1600 °C. Experiments at slightly lower *P-T* conditions also produced some YO, but X-ray diffraction (XRD) powder patterns from the resulting pellet included impurities, precursor Y_2O_3 in the high pressure monoclinic structure (see supplementary material), and a slightly larger lattice parameter than observed in the pure phase. The YO quenched from high pressure is gold in color, has a metallic luster, and crystallizes in the rock salt structure (**Figure 1**), similar to previous syntheses of other REO at high pressure in the 1980s[9] and in agreement with band calculations, which also indicates a gold color, based on low plasma frequency and low free electron density, for the slightly oxygen deficient stoichiometry used in synthesis (**Figure 4**).

The average refined lattice parameter for YO is 4.872 ± 0.008 Å, with a molar volume of 17.41 ± 0.08 cm^3. This is only slightly larger than our DFT calculation, showing a lattice constant of 4.852 Å at room temperature and ambient pressure. The uncertainty is the standard deviation of these values only from experiments in which essentially pure YO was synthesized. For previous work on thin films, the reported lattice constant is 4.936–4.977 Å[16], which is substantially larger than all syntheses at high pressure, but also represents a tetragonal distortion of the rock salt structure. Lattice parameters for bulk YO are presented with bulk and thin film REO from previous work in **Figure 5**. The lattice parameter for YO aligns well with the trend observed in other REO.

The thermochemistry of high pressure materials and rare earth oxides has previously been evaluated using high temperature oxide melt solution calorimetry[1,49–51]. In this process, the sample is dropped from room temperature into a molten solvent at high temperature (in this case sodium molybdate $3Na_2O{\cdot}MoO_4$ at 800 °C) in a twin Calvet-type calorimeter[47,52] and the measured heats of drop solution are used to determine formation enthalpy from elements and/or oxide constituents. For YO, a large variation in dissolution enthalpy was observed across several drops. Furthermore, the enthalpy of formation of YO from Y + Y_2O_3 appeared strongly exothermic, in contrast to the endothermic value obtained by DFT (see data in supplementary **Table S6**). These observations suggest that the YO decomposed during the seconds it took it to drop from room temperature into the calorimeter at 800 ºC. Thus, the oxide melt solution calorimetric experiments were unable to

produce accurate values of heat of formation of YO and we concluded that the rapid decomposition required further study and determination of enthalpy of formation by other methods.

To understand the reaction process and determine the thermochemistry of YO, we used a combination of DSC under vacuum and FDSC. When YO was heated under vacuum in a standard DSC, a sharp, irreversible, exothermic peak was observed at ~180 °C. Decomposition is confirmed by comparing the mass and XRD of the sample before and after heating (see supplementary **Figure S2**). The integrated decomposition enthalpy is –35.7 kJ/mol. The uncertainty is estimated at ± 5 % based on previous calibrations and experiments with the instrumentation[53,54] The experimental enthalpy value agrees well with the predicted value of –32.7 kJ/mol for decomposition of YO to a mixture of Y and Y_2O_3 from DFT and lattice dynamics calculations. To show that decomposition happens quickly, we measured heat flow using FDSC, which enables thermal analysis at extremely rapid heating rates. When YO was heated to 700 °C at a rate 1000 °C/s under argon flow, reactions were observed at ~280 °C and 430 °C and are complete in less than 0.5 s from the onset of heating (**Figure 6**). These results indicate a highly metastable material - one which decomposes readily at modest temperatures and in a matter of seconds under a high heating rate. Although we did not pursue quantitative studies of the kinetics of decomposition, it is clear that YO is extremely metastable on heating at ambient pressure.

We determined the Gibbs free energy of the reaction from pressure and the change in molar volume and used it to calculate the *P-T* boundary for the reaction. The synthesis points do not define a reversible phase boundary but they do suggest that this boundary must lie below the points where synthesis was successful. The lowest *P-T* condition at which YO was observed in XRD was 10 GPa and 1400 °C (**Table 1**). If this is taken as a point on the phase boundary, the total Gibbs energy of transformation is given by:

$$\Delta G^{(P,T)} = \Delta G^{\circ}_{RXN} + P\Delta V = 0. \quad \textbf{(1)}$$

Assuming the volume change is constant and using the atomic density of Y and O in the rock salt structure, the change in molar volume for phase boundary is given by:

$$\Delta V = V_{YO} - (V_{Y\,metal} + V_{Y2O3})/3 \quad \textbf{(2)}$$

The volume change calculated from the mean unit cell volume for YO is –4.18 cm^3/mol, consistent with DFT predictions of –4.14 cm^3/mol). The Gibbs energy of the reaction is then:

$$\Delta G^{\circ}_{RXN} = -P\Delta V, \quad \textbf{(3)}$$

at P = 10 GPa, which yields a value of $\Delta G^{\circ}_{RXN} = 41.80$ kJ/mol. Assuming the enthalpy of the reaction is constant, the entropy change of the reaction can be calculated from the decomposition enthalpy from this single P-T point:

$$\Delta G^{\circ}_{RXN} = \Delta H^{\circ}_{RXN} - T\Delta S^{\circ}_{RXN} \quad \textbf{(4)}$$

which yields an entropy change of $\Delta S^{\circ}_{RXN} = -3.65$ J/mol K. Fitting a line with the Clapeyron slope $\Delta S/\Delta V = dP/dT = 8.72\times10^{-4}$ GPa/K gives an estimate of the P-T phase boundary:

$$P(T) = \left(8.72 \times 10^{-4} \frac{GPa}{K}\right) \times T + 8.54 \text{ GPa}, \quad \textbf{(5)}$$

which is plotted with synthesis data in **Figure 7**. The 0 K intercept is in excellent agreement with the DFT predictions of 8.6 GPa at 0 K. The synthesis conditions, heating time, and unit cell volume from XRD are provided in **Table 1**. The stability field for YO defined by the P-T boundary does not reach atmospheric pressure, so YO is metastable at atmospheric conditions at all temperatures and the observed temperature of the exothermic and irreversible decomposition reaction at 180 °C is kinetically driven. On rapid heating with FDSC, there is an increase in the reaction temperature to 280 °C and a decrease in transformation time.

Rates of formation of YO at high pressure and temperature may also be modified by temperature conditions or kinetics. The experiment at 10 GPa and 1200 °C did not yield any YO, however at just 200 °C higher, at 10 GPa and 1400 °C, some YO was present in the XRD pattern, along with monoclinic (*C2/m*) Y_2O_3 and a weak yttrium metal signal. This may suggest the transformation rate becomes slower as temperature decreases or may be indicative of another Y-oxide phase boundary. The tetragonal distortion of thin films synthesized at atmospheric pressure and small refined domain size data from this work (see **Table S3**) could support that hypothesis, but more work is needed to probe the yttrium-oxygen phase space and synthesis kinetics.

These are important results for thermodynamic studies involving highly metastable materials. YO transforms rapidly at temperatures well below the temperature of the molten solvent in drop solution calorimetric experiments, rendering results from these experiments dubious. The combination of standard DSC with fast scanning calorimetry showed not only that the sample decomposed, but also that the reaction occurred on the very short timescale of the drop into the solution calorimeter. For materials which undergo similar rapid transformations, this indicates that normal high temperature solution calorimetric methods may not be suitable for thermodynamic characterization because the final state of the sample when it is dropped into the calorimeter and before it dissolves in the molten solvent is not well defined. For YO, computations guided the

initial synthesis conditions, and allowed us to overcome this challenge by providing a check on results from drop solution calorimetry, and ultimately corroborated DSC measurements.

Superconductivity was also predicted computationally in a previous work for YO with a potentially promising inverse relationship between critical temperature and pressure. Ref Preliminary magnetic experiments (to be published in future work) did not indicate superconductivity down to 2 K in our samples. This is consistent with epitaxially-distorted rock salt YO synthesized as thin films at ambient pressure[16], which also did not show superconductivity. Further experiments on YO and other bulk rare earth monoxides are critical to probe electronic states and to determine optical and electromagnetic properties of bulk REO.

In conclusion, we used first principles calculations to predict the high pressure stability of YO and successfully synthesized it at high pressure and temperature. While YO decomposed on heating and initially presented challenges to thermochemical analysis, we were able to use our theoretical calculations to guide a series of thermochemistry experiments to obtain results in good agreement with predictions. This highlights the importance of coupling theory and experiment and provides a basis for thermochemical analysis of highly metastable materials.

Acknowledgments

This work was supported by the US National Science Foundation under Collaborative Research Awards DMR-2209026 (Arizona State University) and DMR-2209027 (Brown University) with use of Research Computing at Arizona State University and the Extreme Science and Engineering Discovery Environment (XSEDE), supported by the National Science Foundation (ACI-1548562). We acknowledge the use of facilities within the Eyring Materials Center and the Facility for Open Research in a Compressed Environment (FORCE) at Arizona State University. Preliminary magnetic measurements were conducted by Dustin A. Gilbert at University of Tennessee, Knoxville. We thank Ulrich Häussermann, Kyusei Tsuno, Isaac Rhoden, Kristina Lilova, and Tamilarasan Subramani for assistance with experiments and productive discussion surrounding early experimental setup and results.

Author Declarations

The authors declare no competing financial interests.

Supporting information

Tabulated experimental run data, refinement data and parameters, thermochemical cycles for calorimetry, supporting figures, and a crystallographic information file (CIF) are included as supplementary material.

Tables and Figures

Table 1: Parameters and coefficients for the P-T boundary for the reaction $Y + Y_2O_3 = 3YO$ presented in **Figure 6**.

Sample	*P* (GPa)	*T* (°C)	$V_{\text{unit cell}}$ (Å^3)	Time (h)	Comment
YO #1	10	1200	-	2	Mixed phases, YO not produced
YO #7*	10	1400	116.41	1	Short heating, mixed phases, including YO
YO #8	10	1400	114.37	5	Long heating, mixed phases, including YO
YO #6**	13.5	1800	117.00	1.5	Mixed phases, including YO
YO #2	13.5	1600	114.71	2	~pure YO
YO #11^{++}	15	1600	114.70	2	~pure YO

**indicates results after attempted powdering in glovebox and subsequent color change, **indicates anvil failure during experiment (pressure blowout), $^{++}$indicates multiple syntheses of ~pure YO at these conditions. See supplementary data for full table of experiments.*

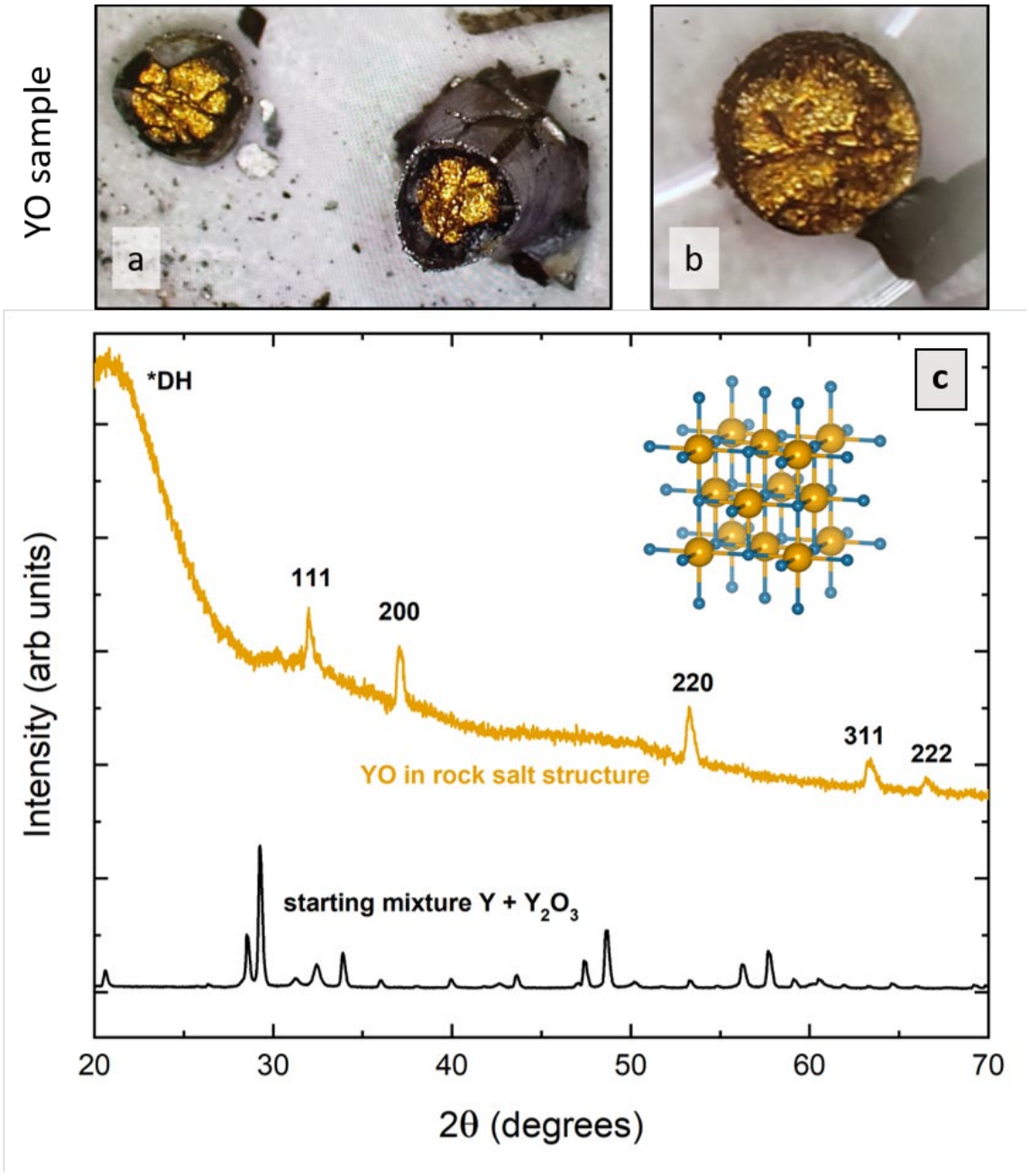

Figure 1: Image of YO in newly-opened high-pressure capsule (a) and the recovered pellet (b) with corresponding XRD patterns (c). Inset in (c) is the rock salt structure from Vesta – gold spheres represent yttrium atoms, blue spheres represent oxygen atoms. YO peaks are indexed to *fcc* symmetry, *DH is the amorphous peak from the domed holder for atmospheric control. YO exhibits an environmentally imposed pellet morphology with gold color and metallic luster. The XRD pattern suggest primarily pure YO, extra peaks are residual from the BN capsule or the Si dome on the controlled atmosphere holder, or small amounts of Y_2O_3 impurity.

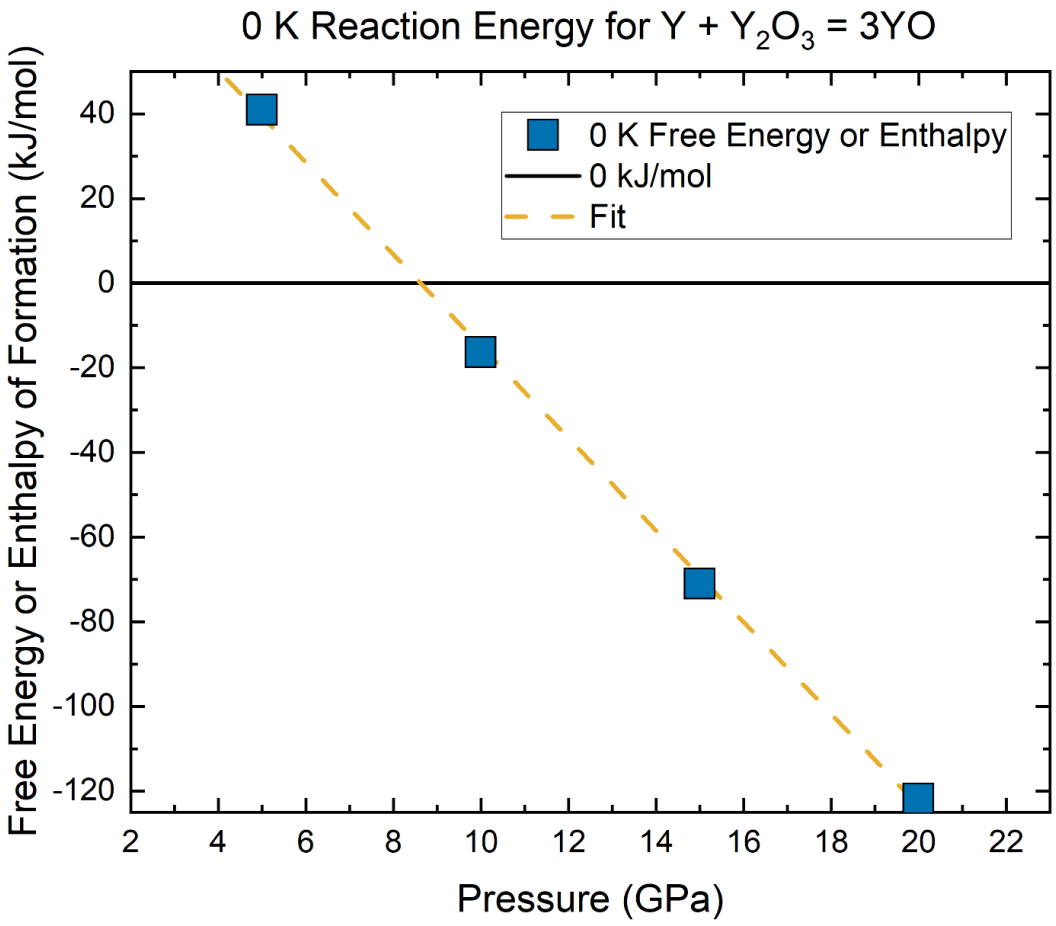

284

285 **Figure 2**: Calculated values of reaction free energy (blue squares) and enthalpy of formation
286 (open circles) at 0 Kelvin for the reaction Y + Y_2O_3 = 3YO from molecular dynamics. The
287 reaction is predicted to occur at 8.6 GPa, when the free energy and enthalpy of reaction are 0 eV.

288

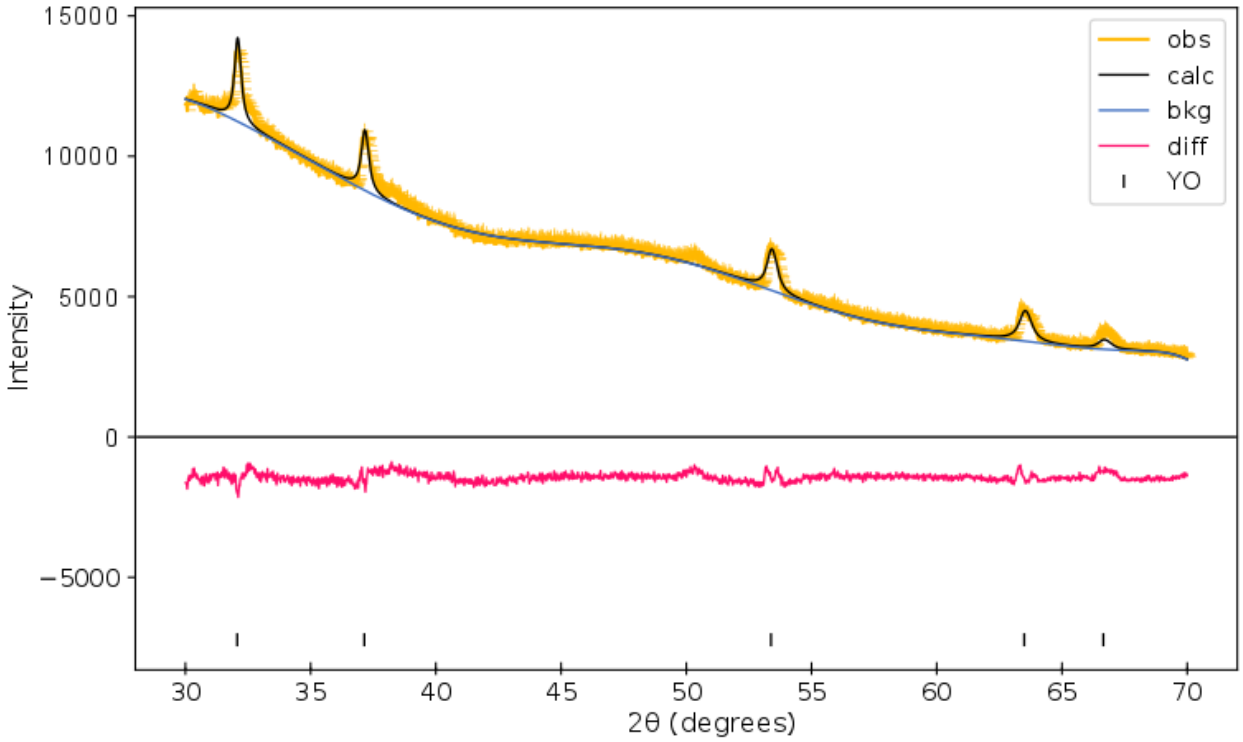

Figure 3 Refinement for YO sample pellet, scanned for 15 hours. Refinement parameters are provided in the supplementary material. The wR value for the refinement is 2.21 %, with a goodness of fit of 1.77.

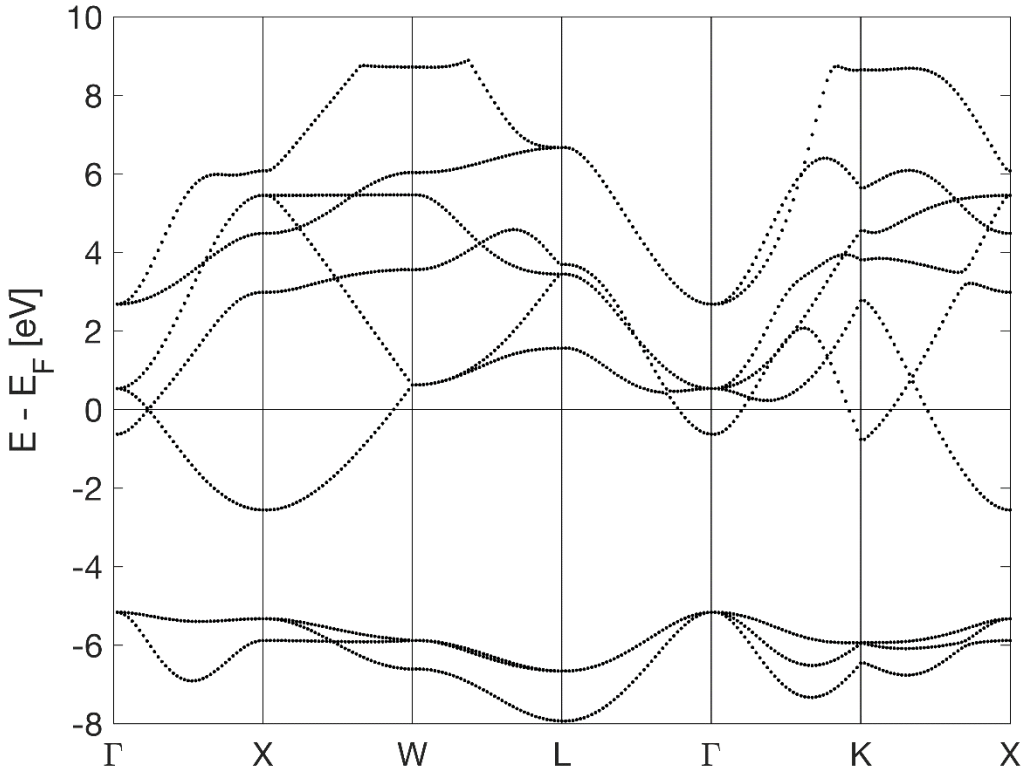

294

295 **Figure 4**: Band structure calculation for YO. The highest occupied band indicates that the one
296 remaining 4d electron of Y^{2+} stays localized in the d orbital, with only a minute portion
297 (approximately 2 %) becoming a free electron gas. As a result, the free electron density is
298 extremely low, leading to an exceptionally low plasma frequency and a golden appearance.

299

300

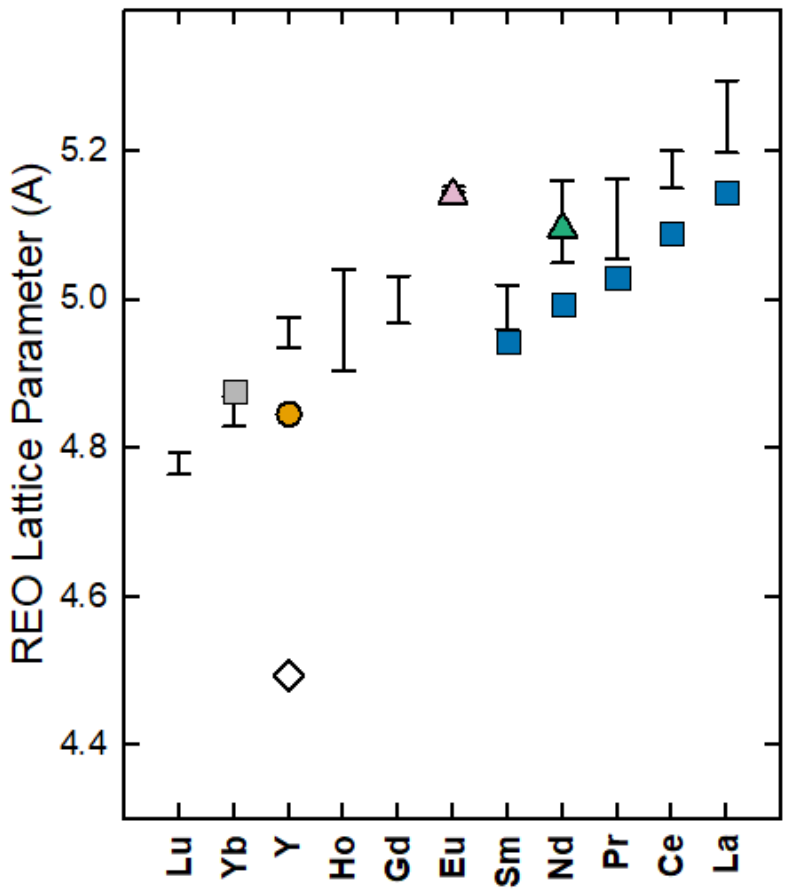

Figure 5 Lattice parameters for REO. Parameters from thin films[14,16,19,21,34,35,55–60] are lines with brackets representing variation in tetragonal distortion due to lattice mismatch, with the exception of EuO, where the brackets represent lattice constants from separate studies. Filled symbols are static high pressure synthesis[9], except EuO (filled pink triangle), which is from the high-temperature reaction of Eu metal and sesquioxide[61], and NdO (filled green triangle), which is from dynamic compression[62]. The open diamond is the recent DFT prediction by Yang, et al., 2021[22]. Refined values for bulk YO (filled gold circle, this work) are smaller than the thin film values like other REO (except Yb and Eu).

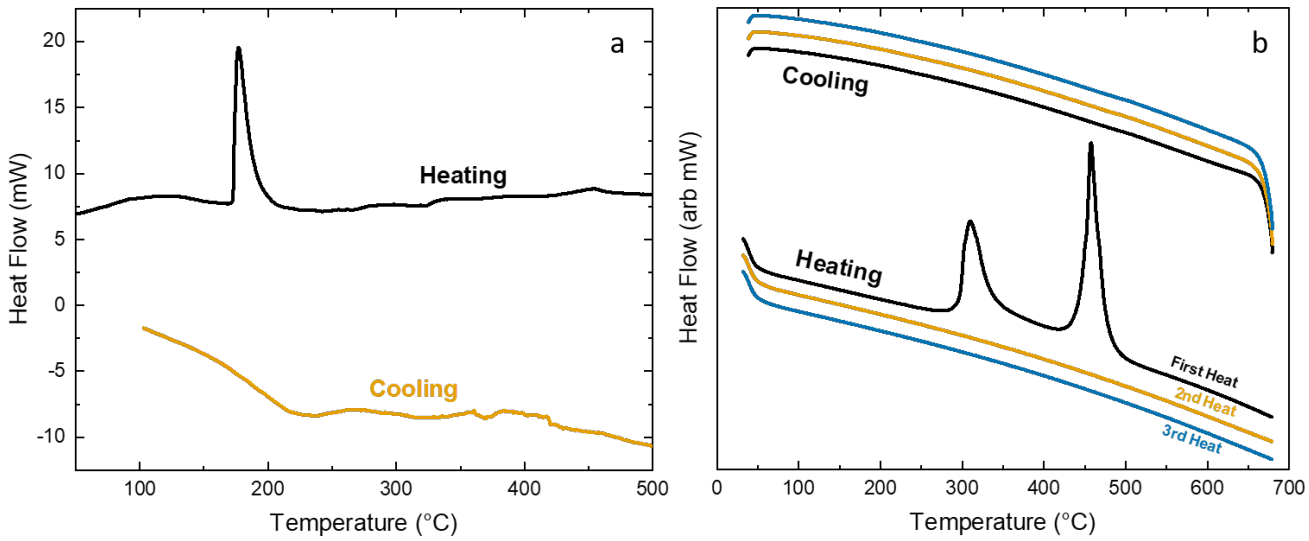

Figure 6: Heat flow in YO measured on a) ASAP/SenSys under vacuum at 10 °C/min and b) the Flash DSC2+ on the high-temperature chip under Ar flow (20 µL/min) heated at 1000 °C/s. All thermal events are irreversible. On the Flash DSC2+, the two peaks probably represent different parts of the sample transforming due to the thermal gradient produced by the Flash chip. Both reactions care complete by around 500 °C, indicating YO transforms in less than 0.5 s.

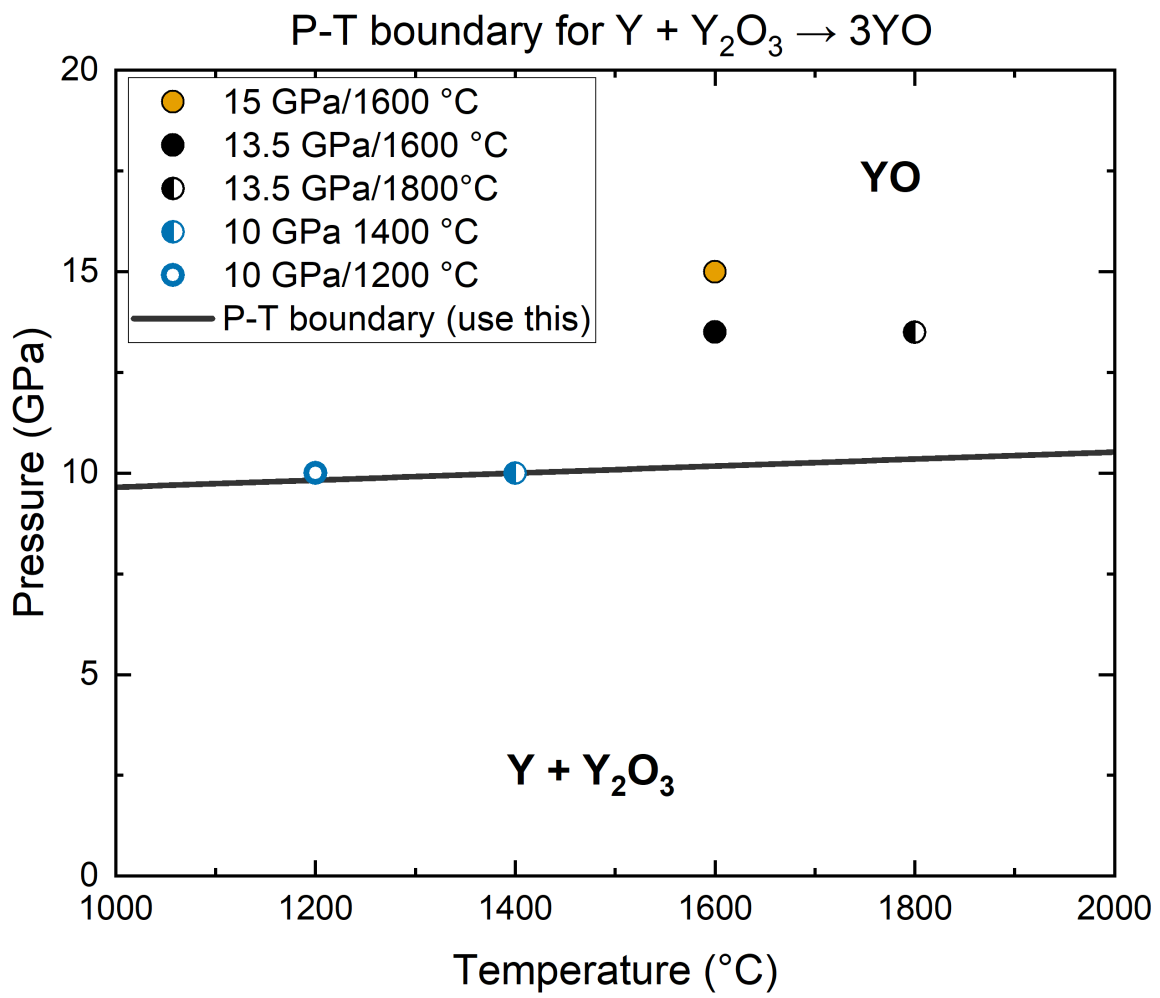

322

323 **Figure 7**: Pressure-temperature synthesis and estimated phase boundary conditions for the
324 reaction Y + Y_2O_3 → 3YO. Closed circles are syntheses of pure YO: 15 GPa and 1600 °C (solid
325 yellow circle), 13.5 GPa and 1600 °C (solid black circle), half-filled circles are syntheses where
326 some YO was present: 13.5 GPa and 1800 °C (half-filled black circle) and 10 GPa and 1400 °C
327 (half-filled blue circle). The open blue circle is the experiment at 10 GPa and 1200 °C, which
328 did not produce YO. The solid black line is the P-T slope, determined from the volume change
329 observed in ~pure YO and entropy calculated from lowest P-T conditions at which YO was
330 produced (half-filled blue circle).

References

(1) Navrotsky, A.; Lee, W.; Mielewczyk-Gryn, A.; Ushakov, S. V.; Anderko, A.; Wu, H.; Riman, R. E. Thermodynamics of Solid Phases Containing Rare Earth Oxides. *J. Chem. Thermodyn.* **2015**, *88*, 126–141. https://doi.org/10.1016/j.jct.2015.04.008.

(2) Fabrichnaya, O.; Seifert, H. J.; Ludwig, T.; Aldinger, F.; Navrotsky, A. The Assessment of Thermodynamic Parameters in the Al2O3-Y2O3 System and Phase Relations in the Y-Al-O System. *Scand. J. Metall.* **2001**, *30* (3), 175–183. https://doi.org/10.1034/j.1600-0692.2001.300308.x.

(3) Wu, M. K.; Ashburn, J. R.; Torng, C. J.; Hor, P. H.; Meng, R. L.; Gao, L.; Huang, Z. J.; Wang, Y. Q.; Chu, C. W. Superconductivity at 93 K in a New Mixed-Phase Y-Ba-Cu-O Compound System at Ambient Pressure. *Phys. Rev. Lett.* **1987**, *58* (9), 908–910. https://doi.org/10.1103/PhysRevLett.58.908.

(4) Chen, D.; Wang, Q.; Liu, Y.; Ning, X. Investigation of Ternary Rare Earth Oxide-Doped YSZ and Its High Temperature Stability. *J. Alloys Compd.* **2019**, *806*, 580–586. https://doi.org/10.1016/j.jallcom.2019.07.198.

(5) Fu, X.; Xu, Y.; Zhou, J. Phase Structure and Vibrational Spectra of Rare-Earth-Oxide Ceramics of Dy2(1−x)Tm2xO3. *J. Mater. Sci.* **2012**, *47* (4), 1697–1701. https://doi.org/10.1007/s10853-011-5948-z.

(6) Brewer, L. *The Thermodynamics of the Rare Earth Oxides*; Contract Report; Lawrence Berkeley National Laboratory: UC Berekeley, 1952; pp 1–6.

(7) Cherepanov, V.; Kolokolov, I.; L'vov, V. The Saga of YIG: Spectra, Thermodynamics, Interaction and Relaxation of Magnons in a Complex Magnet. *Phys. Rep.* **1993**, *229* (3), 81–144. https://doi.org/10.1016/0370-1573(93)90107-O.

(8) Oitmaa, J.; Falk, T. Ferrimagnetism in the Rare-Earth Iron Garnets: A Monte Carlo Study. *J. Phys. Condens. Matter* **2009**, *21* (12), 124212. https://doi.org/10.1088/0953-8984/21/12/124212.

(9) Leger, J. M.; Yacoubi, N.; Loriers, J. Synthesis of Rare Earth Monoxides. *J. Solid State Chem.* **1981**, *36* (3), 261–270. https://doi.org/10.1016/0022-4596(81)90436-9.

(10) Leger, J. M.; Aimonino, P.; Loriers, J.; Dordor, P.; Coqblin, B. Transport Properties of SmO. *Phys. Lett. A* **1980**, *80* (4), 325–327. https://doi.org/10.1016/0375-9601(80)90035-3.

(11) Krill, G.; Ravet, M. F.; Kappler, J. P.; Abadli, L.; Leger, J. M.; Yacoubi, N.; Loriers, C. Magnetic Properties of Some Rare Earth Monoxides LnO (Ln = Pr, Nd, Sm) Mixed Valence State of SmO. *Solid State Commun.* **1980**, *33* (3), 351–353. https://doi.org/10.1016/0038-1098(80)91168-0.

(12) Vedel, I.; Redon, A. M.; Leger, J. M. Pressure-Induced Electronic Instability in CeO. *J. Phys. C Solid State Phys.* **1986**, *19* (19), 3549. https://doi.org/10.1088/0022-3719/19/19/011.

(13) Oliver, M. R.; Dimmock, J. O.; McWhorter, A. L.; Reed, T. B. Conductivity Studies in Europium Oxide. *Phys. Rev. B* **1972**, *5* (3), 1078–1098. https://doi.org/10.1103/PhysRevB.5.1078.

(14) Amrillah, T.; Oka, D.; Shimizu, H.; Sasaki, S.; Saito, D.; Kaminaga, K.; Fukumura, T. Rock Salt-Type HoO Epitaxial Thin Film as a Heavy Rare-Earth Monoxide Ferromagnetic Semiconductor with a Curie Temperature above 130 K. *Appl. Phys. Lett.* **2022**, *120* (8), 082403. https://doi.org/10.1063/5.0081040.

(15) Ushakov, S. V.; Hong, Q.-J.; Gilbert, D. A.; Navrotsky, A.; Walle, A. van de. Thorium and Rare Earth Monoxides and Related Phases. *Materials* **2023**, *16* (4), 1350. https://doi.org/10.3390/ma16041350.

(16) Kaminaga, K.; Sei, R.; Hayashi, K.; Happo, N.; Tajiri, H.; Oka, D.; Fukumura, T.; Hasegawa, T. A Divalent Rare Earth Oxide Semiconductor: Yttrium Monoxide. *Appl. Phys. Lett.* **2016**, *108* (12), 122102. https://doi.org/10.1063/1.4944330.

(17) Arslan, H.; Aulika, I.; Sarakovskis, A.; Bikse, L.; Zubkins, M.; Azarov, A.; Gabrusenoks, J.; Purans, J. Reactive Pulsed Direct Current Magnetron Sputtering Deposition of Semiconducting Yttrium Oxide

Thin Film in Ultralow Oxygen Atmosphere: A Spectroscopic and Structural Investigation of Growth Dynamics. *Vacuum* **2023**, *211*, 111942. https://doi.org/10.1016/j.vacuum.2023.111942.
(18) Lettieri, J.; Vaithyanathan, V.; Eah, S. K.; Stephens, J.; Sih, V.; Awschalom, D. D.; Levy, J.; Schlom, D. G. Epitaxial Growth and Magnetic Properties of EuO on (001) Si by Molecular-Beam Epitaxy. *Appl. Phys. Lett.* **2003**, *83* (5), 975–977. https://doi.org/10.1063/1.1593832.
(19) Kaminaga, K.; Oka, D.; Hasegawa, T.; Fukumura, T. New Lutetium Oxide: Electrically Conducting Rock-Salt LuO Epitaxial Thin Film. *ACS Omega* **2018**, *3* (10), 12501–12504. https://doi.org/10.1021/acsomega.8b02082.
(20) Mauger, A.; Godart, C. The Magnetic, Optical, and Transport Properties of Representatives of a Class of Magnetic Semiconductors: The Europium Chalcogenides. *Phys. Rep.* **1986**, *141* (2), 51–176. https://doi.org/10.1016/0370-1573(86)90139-0.
(21) Kaminaga, K.; Oka, D.; Hasegawa, T.; Fukumura, T. Superconductivity of Rock-Salt Structure LaO Epitaxial Thin Film. *J. Am. Chem. Soc.* **2018**, *140* (22), 6754–6757. https://doi.org/10.1021/jacs.8b03009.
(22) Yang, Q.; Lin, J.; Li, F.; Zhang, J.; Zurek, E.; Yang, G. Pressure-Induced Yttrium Oxides with Unconventional Stoichiometries and Novel Properties. *Phys. Rev. Mater.* **2021**, *5* (4), 044802. https://doi.org/10.1103/PhysRevMaterials.5.044802.
(23) Warf, J. C.; Korst, W. L. *Lanthanum Monoxide*; Studies of the Rare-Earth Hydrides; Technical Report Proj. No. 356-290; Office of Naval Research, Physical Science Division: Los Angeles, Ca, 1956.
(24) Butherus, A. D.; Eick, H. A. Preparation and Some Properties of the Lanthanide Oxide Carbides, Ln4O3C. *J. Am. Chem. Soc.* **1968**, *90* (7), 1715–1718. https://doi.org/10.1021/ja01009a008.
(25) Ellinger, F. H.; Land, C. C.; Cramer, E. M. Extractive and Physical Metallurgy of Plutonium and Its Alloys. *Ed WD Wilkinson Intersci. Publ. N. Y.* **1960**.
(26) Ellinger, F. H. *THE CRYSTAL STRUCTURE OF NEODYMIUM METAL AND OF NEODYMIUM MONOXIDE*; Technical Report; Los Alamos Scientific Lab., 1953; pp 1–11.
(27) Ellinger, F. H.; Zachariasen, W. H. The Crystal Structure of Samarium Metal and of Samarium Monoxide [1]. *J. Am. Chem. Soc.* **1953**, *75* (22), 5650–5652. https://doi.org/10.1021/ja01118a052.
(28) Eick, H. A.; Baenziger, N. C.; Eyring, L. Lower Oxides of Samarium and Europium. The Preparation and Crystal Structure of $SmO_{0.4\text{-}0.6}$, SmO and EuO [1]. *J. Am. Chem. Soc.* **1956**, *78* (20), 5147–5149. https://doi.org/10.1021/ja01601a003.
(29) Achard, J.-C.; Tsoucaris, G. RADIOCRYSTALLOGRAPHIC STUDY OF THE MONOXIDE OF YTTERBIUM. *Compt Rend* **1958**, *246*.
(30) Gschneidner, K. A. Rare Earth Alloys: A Critical Review of the Alloy Systems of the Rare Earth, Scandium, and Yttrium Metals. **1961**.
(31) Felmlee, T. L.; Eyring, L. Ternary System Samarium-Nitrogen-Oxygen and the Question of Lower Oxides of Samarium. *Inorg. Chem.* **1968**, *7* (4), 660–666. https://doi.org/10.1021/ic50062a006.
(32) Leger, J. M.; Yacoubi, N.; Loriers, J. Synthesis of Neodymium and Samarium Monoxides under High Pressure. *Inorg. Chem.* **1980**, 2252–2254.
(33) Morss, L. R.; Konings, R. J. M. Thermochemistry of Binary Rare Earth Oxides. In *Binary Rare Earth Oxides*; Adachi, G., Imanaka, N., Kang, Z. C., Eds.; Kluwer Academic Publishers: Dordrecht, 2005; pp 163–188. https://doi.org/10.1007/1-4020-2569-6_7.
(34) Saito, D.; Kaminaga, K.; Oka, D.; Fukumura, T. Itinerant Ferromagnetism in Rocksalt NdO Epitaxial Thin Films. *Phys. Rev. Mater.* **2019**, *3* (6), 064407. https://doi.org/10.1103/PhysRevMaterials.3.064407.
(35) Shimizu, H.; Oka, D.; Kaminaga, K.; Saito, D.; Yamamoto, T.; Abe, N.; Kimura, N.; Shiga, D.; Kumigashira, H.; Fukumura, T. Rocksalt-Type PrO Epitaxial Thin Film as a Weak Ferromagnetic Kondo Lattice. *Phys. Rev. B* **2022**, *105* (1), 014442. https://doi.org/10.1103/PhysRevB.105.014442.

(36) Huber, E. J.; Head, E. L.; Holley, C. E. The Heat of Combustion of Yttrium. *J. Phys. Chem.* **1957**, *61* (4), 497–498. https://doi.org/10.1021/j150550a027.
(37) Hohenberg, P.; Kohn, W. Inhomogeneous Electron Gas. *Phys. Rev.* **1964**, *136* (3B), B864–B871. https://doi.org/10.1103/PhysRev.136.B864.
(38) Kohn, W.; Sham, L. J. Self-Consistent Equations Including Exchange and Correlation Effects. *Phys. Rev.* **1965**, *140* (4A), A1133–A1138. https://doi.org/10.1103/PhysRev.140.A1133.
(39) Kresse, G.; Furthmüller, J. Efficiency of Ab-Initio Total Energy Calculations for Metals and Semiconductors Using a Plane-Wave Basis Set. *Comput. Mater. Sci.* **1996**, *6* (1), 15–50. https://doi.org/10.1016/0927-0256(96)00008-0.
(40) Kresse, G.; Furthmüller, J. Efficient Iterative Schemes for *Ab Initio* Total-Energy Calculations Using a Plane-Wave Basis Set. *Phys. Rev. B* **1996**, *54* (16), 11169–11186. https://doi.org/10.1103/PhysRevB.54.11169.
(41) Blöchl, P. E. Projector Augmented-Wave Method. *Phys. Rev. B* **1994**, *50* (24), 17953–17979. https://doi.org/10.1103/PhysRevB.50.17953.
(42) Perdew, J. P.; Burke, K.; Ernzerhof, M. Generalized Gradient Approximation Made Simple. *Phys. Rev. Lett.* **1996**, *77* (18), 3865–3868. https://doi.org/10.1103/PhysRevLett.77.3865.
(43) van de Walle, A.; Asta, M.; Ceder, G. The Alloy Theoretic Automated Toolkit: A User Guide. *Calphad* **2002**, *26* (4), 539–553. https://doi.org/10.1016/S0364-5916(02)80006-2.
(44) Leinenweber, K. D.; Tyburczy, J. A.; Sharp, T. G.; Soignard, E.; Diedrich, T.; Petuskey, W. B.; Wang, Y.; Mosenfelder, J. L. Cell Assemblies for Reproducible Multi-Anvil Experiments (the COMPRES Assemblies). *Am. Mineral.* **2012**, *97* (2–3), 353–368. https://doi.org/10.2138/am.2012.3844.
(45) Toby, B. H.; Von Dreele, R. B. GSAS-II: The Genesis of a Modern Open-Source All Purpose Crystallography Software Package. *J. Appl. Crystallogr.* **2013**, *46* (2), 544–549. https://doi.org/10.1107/S0021889813003531.
(46) Jain, A.; Ong, S. P.; Hautier, G.; Chen, W.; Richards, W. D.; Dacek, S.; Cholia, S.; Gunter, D.; Skinner, D.; Ceder, G.; Persson, K. A. Commentary: The Materials Project: A Materials Genome Approach to Accelerating Materials Innovation. *APL Mater.* **2013**, *1* (1), 011002. https://doi.org/10.1063/1.4812323.
(47) Navrotsky, A. Progress and New Directions in High Temperature Calorimetry Revisited. *Phys. Chem. Miner.* **1997**, *24* (3), 222–241. https://doi.org/10.1007/s002690050035.
(48) Navrotsky, A. Progress and New Directions in Calorimetry: A 2014 Perspective. *J. Am. Ceram. Soc.* **2014**, *97* (11), 3349–3359. https://doi.org/10.1111/jace.13278.
(49) Ito, E.; Akaogi, M.; Topor, L.; Navrotsky, A. Negative Pressure-Temperature Slopes for Reactions Formign $MgSiO_3$ Perovskite from Calorimetry. *Science* **1990**, *249* (4974), 1275–1278. https://doi.org/10.1126/science.249.4974.1275.
(50) Akaogi, M.; Ross, N. L.; McMillan, P.; Navrotsky, A. The Mg2SiO4 Polymorphs (Olivine, Modified Spinel and Spinel)–Thermodynamic Properties from Oxide Melt Solution Calorimetry, Phase Relations, and Models of Lattice Vibrations | American Mineralogist | GeoScienceWorld. *Am. Mineral.* **1984**, *69*, 499–512.
(51) Navrotsky, A.; Akaogi, M. The α, β, γ Phase Relations in Fe_2SiO_4-Mg_2SiO_4 and Co_2SiO_4-Mg_2SiO_4 : Calculation from Thermochemical Data and Geophysical Applications. *J. Geophys. Res. Solid Earth* **1984**, *89* (B12), 10135–10140. https://doi.org/10.1029/JB089iB12p10135.
(52) Navrotsky, A. Progress and New Directions in High Temperature Calorimetry. *Phys. Chem. Miner.* **1977**, *2* (1–2), 89–104. https://doi.org/10.1007/BF00307526.
(53) Ushakov, S. V.; Navrotsky, A. Direct Measurements of Water Adsorption Enthalpy on Hafnia and Zirconia. *Appl. Phys. Lett.* **2005**, *87* (16), 164103. https://doi.org/10.1063/1.2108113.

(54) Ushakov, S. V.; Navrotsky, A. Supplementary Material for Direct Measurements of Water Adsorption Enthalpy on Hafnia and Zirconia. *Appl. Phys. Lett.* **2005**, *87* (16), 164103. https://doi.org/10.1063/1.2108113.
(55) Yamamoto, T.; Kaminaga, K.; Saito, D.; Oka, D.; Fukumura, T. High Electron Mobility with Significant Spin-Orbit Coupling in Rock-Salt YbO Epitaxial Thin Film. *Appl. Phys. Lett.* **2019**, *114* (16), 162104. https://doi.org/10.1063/1.5085938.
(56) Yamamoto, T.; Kaminaga, K.; Saito, D.; Oka, D.; Fukumura, T. Rock Salt Structure GdO Epitaxial Thin Film with a High Ferromagnetic Curie Temperature. *Appl. Phys. Lett.* **2020**, *117* (5), 052402. https://doi.org/10.1063/5.0017954.
(57) Uchida, Y.; Kaminaga, K.; Fukumura, T.; Hasegawa, T. Samarium Monoxide Epitaxial Thin Film as a Possible Heavy-Fermion Compound. *Phys. Rev. B* **2017**, *95* (12), 125111. https://doi.org/10.1103/PhysRevB.95.125111.
(58) Abe, N.; Oka, D.; Kaminaga, K.; Shiga, D.; Saito, D.; Yamamoto, T.; Kimura, N.; Kumigashira, H.; Fukumura, T. Rocksalt CeO Epitaxial Thin Film as a Heavy-Fermion System Transiting from p-Type Metal to Partially Compensated n-Type Metal by $4f$ Delocalization. *Phys. Rev. B* **2022**, *106* (12), 125106. https://doi.org/10.1103/PhysRevB.106.125106.
(59) Veronica, G.; Link to external site, this link will open in a new tab; Held, R.; Bousquet, E.; Link to external site, this link will open in a new tab; Yakun, Y.; Melville, A.; Zhou, H.; Link to external site, this link will open in a new tab; Venkatraman, G.; Link to external site, this link will open in a new tab; Phillipe, G.; Spaldin, N. A.; Link to external site, this link will open in a new tab; Schlom, D. G.; Link to external site, this link will open in a new tab; Stanislav, K.; Link to external site, this link will open in a new tab. Making EuO Multiferroic by Epitaxial Strain Engineering. *Commun. Mater.* **2020**, *1* (1). https://doi.org/10.1038/s43246-020-00075-1.
(60) Miyazaki, H.; Im, H. J.; Terashima, K.; Yagi, S.; Kato, M.; Soda, K.; Ito, T.; Kimura, S. La-Doped EuO: A Rare Earth Ferromagnetic Semiconductor with the Highest Curie Temperature. *Appl. Phys. Lett.* **2010**, *96* (23), 232503. https://doi.org/10.1063/1.3416911.
(61) Shafer, M. W.; Torrance, J. B.; Penney, T. Relationship of Crystal Growth Parameters to the Stoichiometry of EuO as Determined by I.R. and Conductivity Measurements. *J. Phys. Chem. Solids* **1972**, *33* (12), 2251-IN1. https://doi.org/10.1016/S0022-3697(72)80299-3.
(62) Batsanov, S. S. Inorganic Chemistry of High Dynamic Pressures. *Russ. Chem. Rev.* **1986**, *55* (4), 297–315. https://doi.org/10.1070/RC1986v055n04ABEH003191.